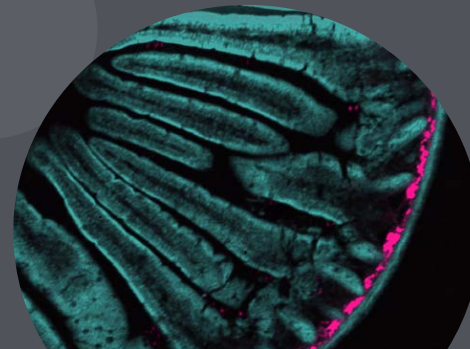
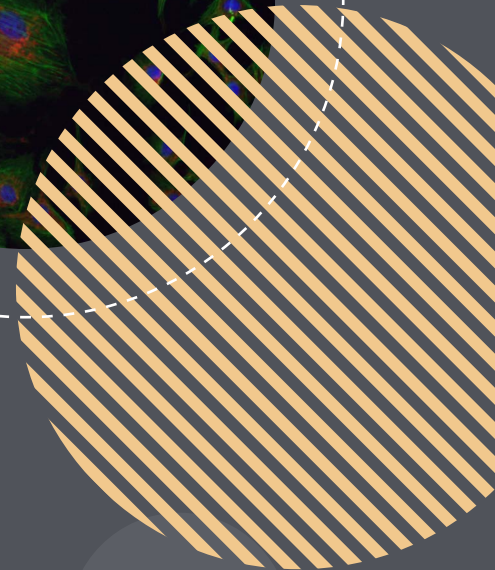
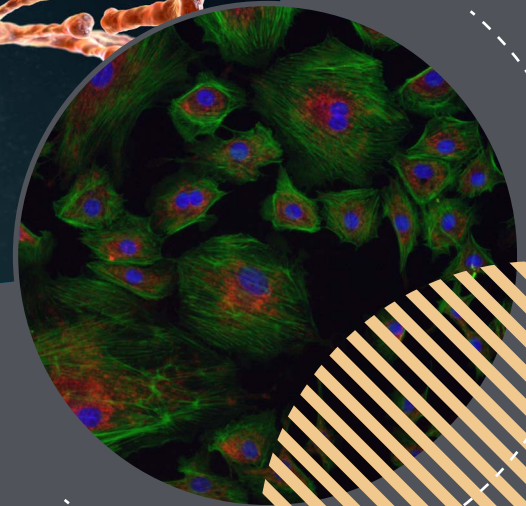
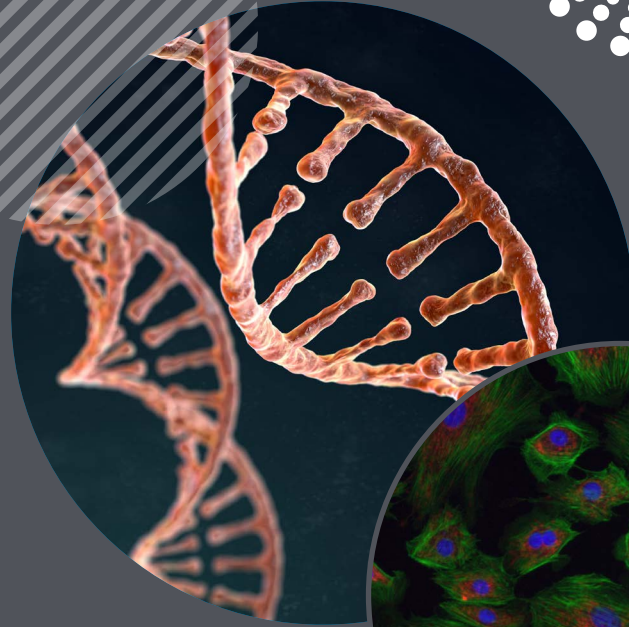
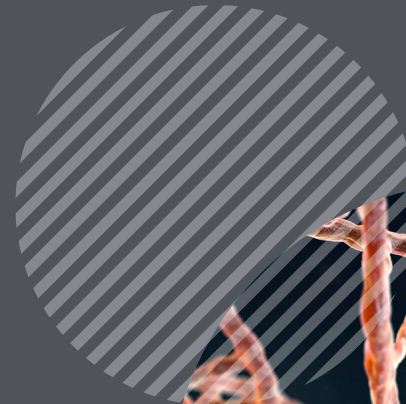




EDINBURGH  
INSTRUMENTS

# Bioscience Applications

eBook Series



# Contents

---

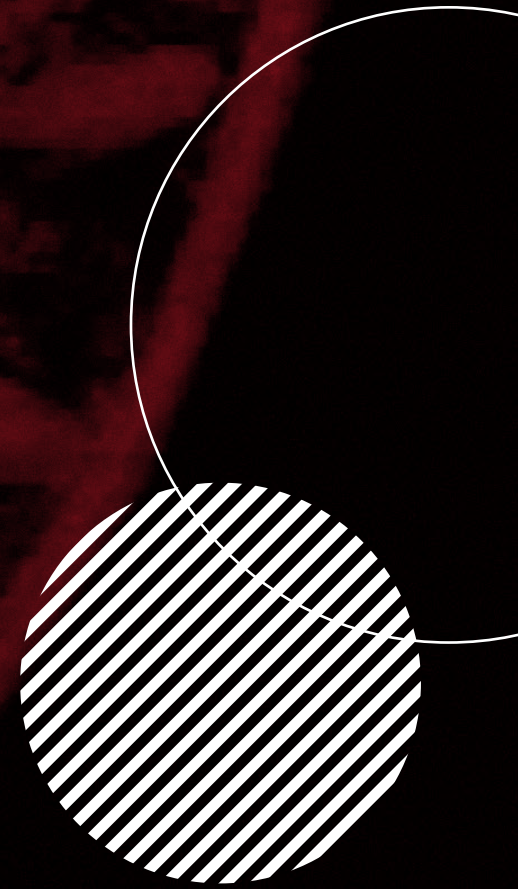
Multiphoton Imaging of Mouse Intestine	3
Discrimination of Bacteria Species Using Raman Microscopy	6
Fluorescence Microscopy with the FS5 Spectrofluorometer	9
Molecular Beacon Probe Fluorescent Detection of DNA	13
ATR-FTIR of Blood Serum	17

---

# Multiphoton Imaging of Mouse Intestine

## Key Highlights

- Two-photon techniques to study biological samples: 2PEF & SHG.
- Femtosecond laser and CCD camera for spectral 2PEF & SHG.
- Femtosecond laser with pulse picker, TCSPC electronics, and hybrid photodetector for 2PEF lifetime.



## Multiphoton Imaging of Mouse Intestine

Two-photon excited fluorescence (2PEF) and second harmonic generation (SHG) are complementary multiphoton imaging techniques for studying biological samples. Both imaging techniques utilise femtosecond pulsed infrared excitation light to generate shorter wavelength light to image the sample but operate via fundamentally different physical processes

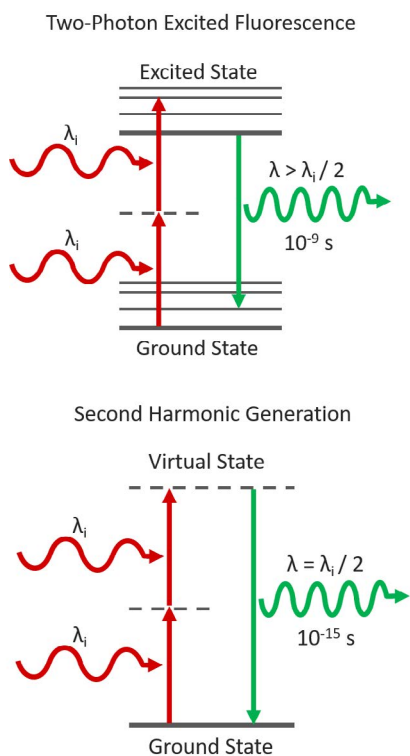


Figure 1: Two-Photon Excited Fluorescence vs Second Harmonic Generation.

(Figure 1). In 2PEF, two infrared photons are simultaneously absorbed by a fluorophore promoting it to an excited state which then radiatively relaxes emitting shorter wavelength fluorescence.

In contrast, SHG is not an absorption and emission process and instead the two infrared photons combine in a non-linear optical material with a particular symmetry to generate a new photon with exactly half the wavelength of the incident photons. Both techniques take advantage of the lower scattering and absorption of infrared light to enable imaging deep into tissue. In this application note, an Edinburgh Instruments RMS1000 Confocal Raman Microscope is used to image a tissue section of mouse intestine using 2PEF and SHG microscopy.

### Experimental Configuration

The sample to be imaged was a section of mouse intestine tissue stained with Alexa Fluor® 568. The RMS1000 was equipped with a motorised XYZ stage and a 40x NA = 0.75 objective. For spectral imaging the RMS1000 was equipped with a back-illuminated CCD camera and for lifetime imaging; a photon counting Hybrid Photodetector and time-correlated single photon counting (TCSPC) electronics. 2PEF and SHG both require a very high excitation intensity, which is achieved using a mode-locked femtosecond pulsed laser. The RMS1000 has external laser coupling ports that enable the optical coupling of femtosecond lasers into the microscope. The optical setup for the femtosecond excitation source is shown in Figure 2. The laser was a Chromacity 1040 HP femtosecond fibre laser with an output wavelength of 1040 nm and an

80 MHz repetition rate (Chromacity Ltd., UK). For lifetime imaging the output of the laser was pulse picked to the desired pulse frequency using a pulseSelect pulse picker (APE GmbH, Germany). A small fraction of the pulse picker output was picked-off into an Edinburgh Instruments OT900 optical trigger module to trigger the TCSPC electronics. For spectral measurements, the pulse picker was bypassed, and the 80 MHz laser output coupled directly into the RMS1000.

### 2PEF & SHG Spectral Imaging with CCD Camera

The intestine tissue section was first imaged spectrally using the CCD camera of the RMS1000. A  $900 \mu\text{m} \times 800 \mu\text{m}$  area of the sample was mapped with a spatial resolution of  $2 \mu\text{m}$ . The sample was excited at 1040 nm 80 MHz and the 2PEF and SHG

signals acquired simultaneously using the CCD camera. The resulting multiphoton image is shown in Figure 3a. 2PEF at 630 nm from the Alexa Fluor® 568 dye is shown in teal and reveals the structure of the intestinal villi. The area shown in pink is SHG at 520 nm from fibrillar collagen near the intestinal wall. SHG only occurs from molecular structures that are non-centrosymmetric and fibrillar collagen is a common biological structure with this property, eliciting a strong SHG response. Each point in the image has a corresponding spectrum, and the spectra at two points A and B are shown in Figure 3b. At point A there is only 2PEF from the Alexa Fluor® 568 dye which has a broad emission centred at 630 nm, while at point B there is an additional sharp peak at 520 nm which is the SHG signal. The colour image in Figure 3a was obtained by plotting the intensity of the spectra at 630 nm and 520 nm for 2PEF and SHG respectively.

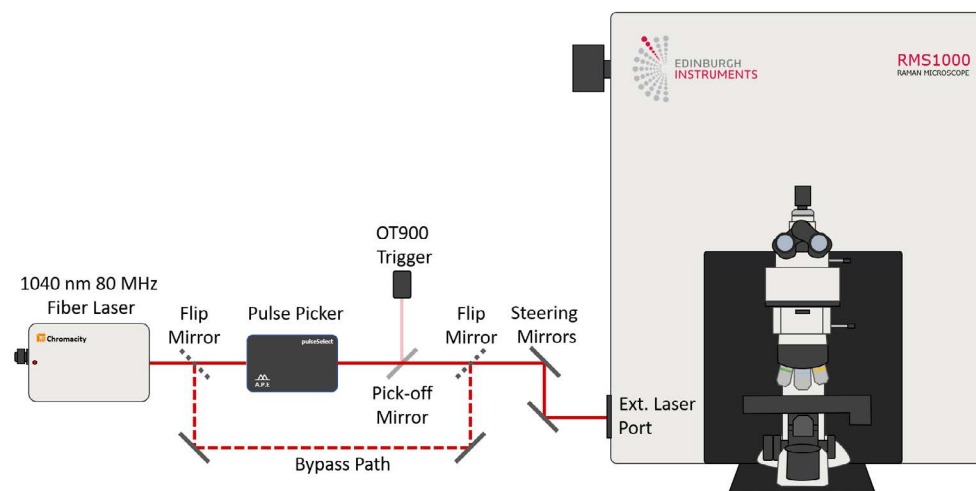


Figure 2: Optical setup for 2PEF and SHG microscopy with the Edinburgh Instruments RMS1000.

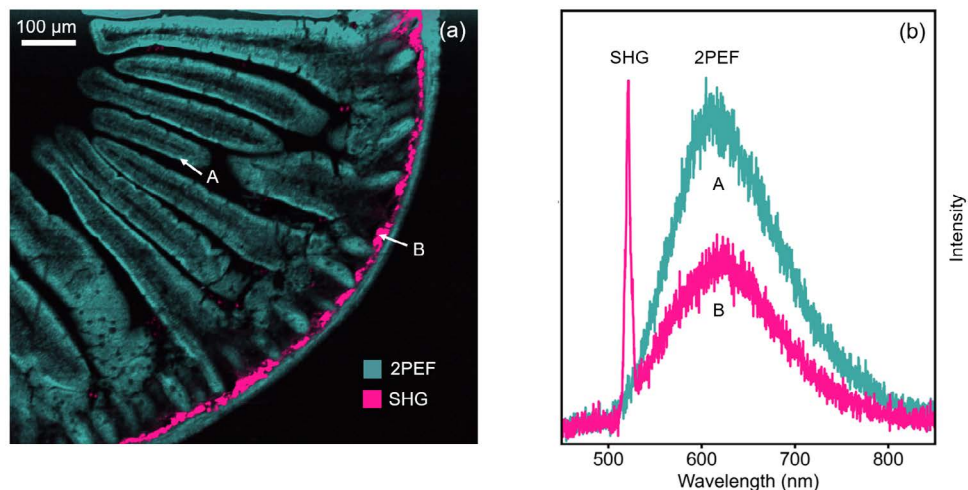


Figure 3: (a) 2PEF and SHG image of mouse intestine section stained with Alexa Fluor<sup>®</sup> 568 and (b) extracted spectra from two points in the image.

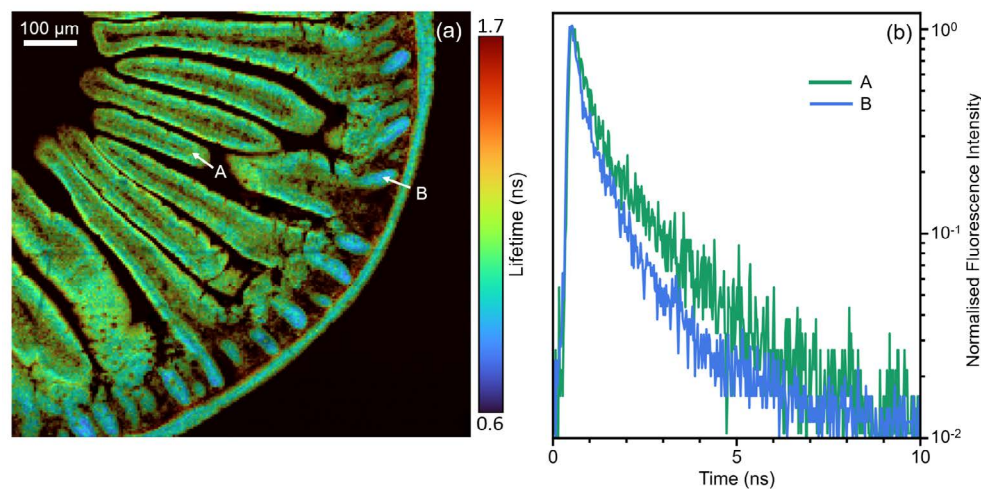


Figure 4: (a) 2PEF lifetime image of mouse intestine section stained with Alexa Fluor<sup>®</sup> 568 and (b) extracted fluorescence decays from two points in the image.

## 2PEF Lifetime Imaging with Hybrid Photodetector

Additional information can be obtained by two-photon fluorescence lifetime imaging. For lifetime imaging the repetition rate of the laser was lowered to 20 MHz using the pulse picker to ensure complete fluorescence decay between pulses. The same 900 μm x 800 μm area was mapped and the fluorescence decay at each point recorded using TCSPC on the photon counting Hybrid Photodetector. Each fluorescence decay was fit with an exponential model using the RMS1000 Ramacle<sup>®</sup> software and the resulting lifetime image is shown in Figure 4a. The lifetime image shows a decreased fluorescence lifetime in the intestinal crypts near the intestinal wall compared with the villi; an example of the increased information that can routinely be obtained from lifetime imaging.

## Conclusion

A section of mouse intestine was imaged using multiphoton microscopy with the RMS1000 Confocal Raman microscope. The RMS1000 can be equipped with an external femtosecond laser and TCSPC lifetime electronics for advanced spectral and time-resolved multiphoton imaging techniques such as 2PEF and SHG which augments its core Raman imaging capability.

# Discrimination of Bacteria Species Using Raman Microscopy



## Key Highlights

- Identifying different bacterial species is essential for patient care.
- Conventional techniques are resource-intensive and time-consuming.
- Raman spectroscopy, coupled with machine learning, can rapidly identify bacterial species.

# Discrimination of Bacteria Species Using Raman Microscopy and Principal Component Analysis

## Introduction

The rapid and accurate identification of specific bacterial species and strains is crucial for administering the correct treatment and preventing the acceleration of antimicrobial resistance.<sup>1</sup> Despite being highly effective and reliable, conventional gold standard techniques, such as polymerase chain reaction and enzyme-linked immunosorbent assay, are resource-intensive and time-consuming.

Additionally, they require skilled personnel and often prior knowledge of the bacteria under investigation, limiting their potential for point-of-use applications in a clinical setting.<sup>2</sup> An alternative technique that has the potential to offer rapid identification is Raman spectroscopy because of the information-rich data it provides and the ability of the technique to be coupled with multivariate analysis (MVA) and machine learning approaches. In this Application Note, an Edinburgh Instruments RM5 Raman Microscope is combined with the multivariate technique principal component analysis (PCA) to discriminate between bacterial species.<sup>3</sup>

## Materials and Methods

*Bacillus subtilis* (*B. subtilis*), *Clostridium sporogenes* (*C. sporogenes*), and *Escherichia coli* (*E. coli*) were purchased

from NCIMB. Each species was individually cultured on horse blood agar for 24 hours at 37°C. Biomass from the cultures was collected and washed three times in deionised water to prevent spectral interference from the agar. The resulting slurries were transferred onto calcium fluoride (CaF<sub>2</sub>) slides and left to dry before being analysed.



Figure 1: Edinburgh Instruments RM5 Raman Microscope.

Raman microscopy was performed on the samples using an RM5 equipped with a 532 nm laser, a 1200 gr/mm diffraction grating, and a back-illuminated CCD camera, Figure 1. Datasets were exported to Eigenvector Solo® software for PCA analysis.

## Raman Spectral Analysis of Bacteria

The two species initially analysed were *E. coli* and *B. subtilis*. *E. coli* is a predominant species that causes extraintestinal illness in humans, such as urinary tract infections, pneumonia, and meningitis. *B. subtilis*, while not considered pathogenic to humans, is in the same genus as *B. anthracis*, the species

responsible for anthrax. The two species were first analysed using Raman spectral analysis, Figure 2. One hundred spectra were recorded from different points across each colony. Then, each spectrum was fit with the same background correction algorithm and maximum-minimum normalisation, which corrects for any sample and experimental variables such as thickness and density without significantly altering spectral features.<sup>4</sup>

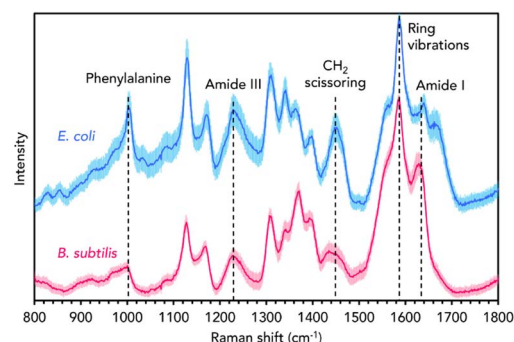


Figure 2: Raman spectra of *B. subtilis* (red) and *E. coli* (blue).

The solid blue and red lines represent the mean spectra from each 100-spectrum dataset, and the surrounding shaded curves represent the  $\pm$  standard deviation.

Both spectra contain the archetypical vibrational fingerprints of biological materials, such as the band attributable to the amino acid phenylalanine at 1001 cm<sup>-1</sup>, the amide III and I bands at 1250 cm<sup>-1</sup> and 1640 cm<sup>-1</sup>, the CH<sub>2</sub> scissoring band at 1450 cm<sup>-1</sup>, and the sharp band at 1580 cm<sup>-1</sup> which can be assigned to aromatic ring vibrations from nucleic acid bases.<sup>5</sup> Subtle differences between the two species can be observed, including the relative intensities, positions,

and shapes of various bands within the mean spectra. The Raman spectra of bacteria are information-rich and, under the correct experimental conditions and with appropriate data pre-processing, can be used to discriminate between species and even strains based on differences in their chemical composition.

## PCA for Bacterial Discrimination

When detecting bacterial infections in a clinical setting, discriminating different species and administering specific treatments is crucial because the incorrect use of antimicrobial drugs causes antimicrobial resistance. A manual comparison of the statistically significant number of Raman spectra required for strain and species delineation is impractical, time-consuming, and unreliable. Therefore, Raman spectra are standardly analysed with MVA techniques that enable the categorisation of samples into different groups based on the spectral variance and chemical information they exhibit.

One MVA technique frequently used alongside Raman spectroscopy is PCA.<sup>6</sup> This powerful dimensionality reduction technique reduces spectra into a defined number of principal components (PCs), which only retain information about the key variables causing variance across the dataset. It is an unsupervised technique that finds patterns in datasets and is excellent for exploratory data analysis. The output of PCA is an easily interpretable cluster plot in which each measurement from the dataset is a point, and the relative position (scores) of each point within the plot infers differences in the spectral output and, therefore, chemical composition.

PCA was performed on the combined spectral datasets to discriminate between the *E. coli* and *B. subtilis* samples, Figure 3.

The PCA score plot in Figure 3a shows that the two samples were well separated and hence discriminated effectively based on their spectral features. Separation between the two bacteria was observed in the first PC (PC1), which is the PC that gives rise to the highest level of spectral variance (86.71%) from across the dataset. Only one PC was needed to separate the species in this instance, but for more complex examples PCA scores plots can be two or three dimensional and include any combination of PCs.

The PCA scores for each spectrum in the dataset are linked to corresponding PC loadings, shown in Figure 3b for PC1. For spectral datasets, the PC loading plot appears as a spectrum which can have positive and negative peaks. The loading plot indicates that the *E. coli* spectra cluster positively in PC1 because of features such as the bands attributable to phenylalanine, the amide III vibration, and the CH<sub>2</sub> scissoring mode, which are all positive in the loading plot. The *B. subtilis* clusters negatively in PC1 because the features that dominate the *E. coli* spectra are diminished proportionately to the much more intense aromatic ring vibration band, which is negative in the loading plot.

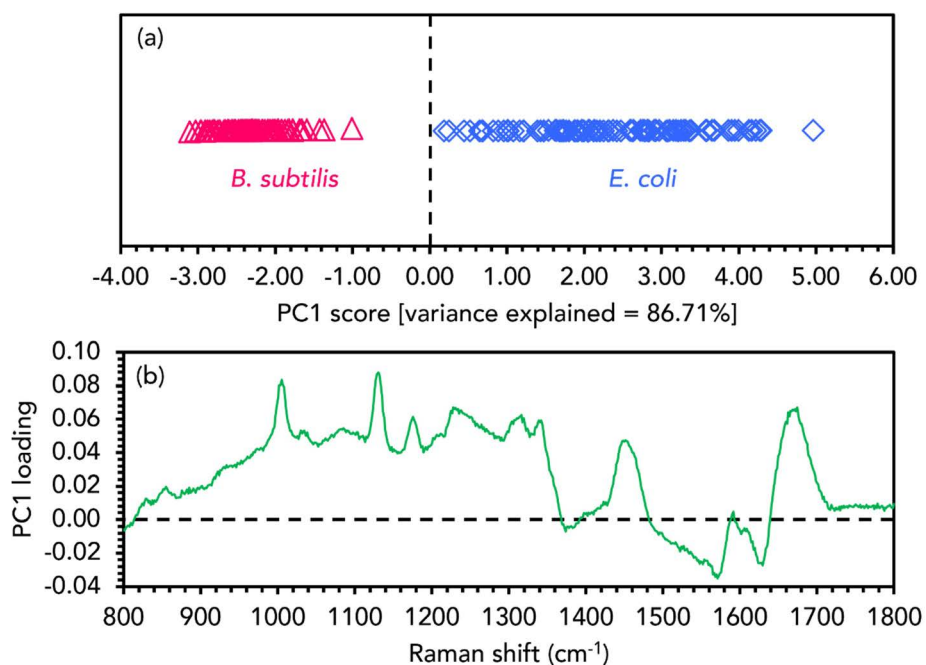


Figure 3: PCA discrimination of *B. subtilis* (red) and *E. coli* (blue).

## PCA Imaging of Bacterial Colonies

PCA can also be used to generate images showing the location of different species. PC scores contain information about the entire Raman spectrum from each imaging pixel, which means that components within samples with very subtle spectral differences can be discriminated within the image.

To demonstrate this, *E. coli* and *C. sporogenes*, a species abundant in the human microbiome that can cause endogenous infections, were added to the same CaF<sub>2</sub> slide. A Raman map was taken across the interface between colonies of the two species. PCA was performed on the Raman mapping dataset, in which each spectrum was baseline corrected using the same Savitsky-Golay filter and maximum-minimum normalised, and images were constructed using PC1 scores, Figures 4. The image demonstrates that the two species could be spatially distinguished using their clustering in PC1, because it shows an evident change in the spectral signatures exhibited on either side of the interface.

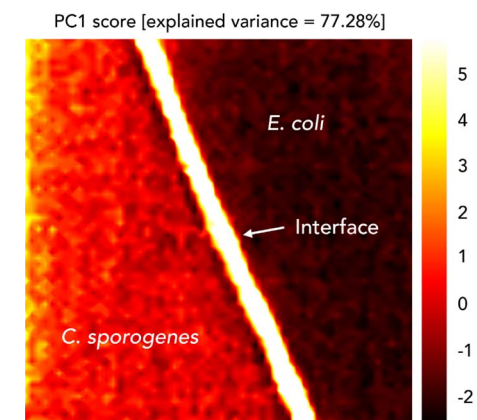


Figure 4: PCA image of the interface between *C. sporogenes* and *E. coli* colonies overlapping.

## References

1. M. E. Berry *et al.*, Surface enhanced Raman scattering for the multiplexed detection of pathogenic organisms: towards point-of-use applications, *Analyst*, 2021, **146**, 6084-6101.
2. J.-C. Lagier *et al.*, Current and Past Strategies for Bacterial Culture in Clinical Microbiology, *Clin. Microbiol. Rev.*, 2015, **28**, 208-236.
3. C.-S. Ho *et al.*, Rapid identification of pathogenic bacteria using Raman spectroscopy and deep learning, *Nat. Commun.*, 2019, **10**, 4927.
4. H. J. Butler *et al.*, Using Raman spectroscopy to characterize biological materials, *Nat. Protoc.*, 2016, **11**, 664-687.
5. S. A. Strola *et al.*, Single bacteria identification by Raman spectroscopy, *J. Biomed. Opt.*, 2014, **19**, 111610.
6. A. Dita *et al.*, Principal Components Analysis of Raman Spectral Data for Screening of Hepatitis C Infection, *Spectrochim. Acta A*, **221**, 117173.



# Fluorescence Microscopy with the FS5 Spectrofluorometer

## Key Highlights

- Fluorescence microscopy is an imaging technique that uses fluorescence to provide contrast to microscope images.
- In biomedical imaging it offers a high degree of specificity and selectivity.
- Fluorophore labelling allows cellular structures to be imaged.

## Fluorescence Microscopy with the FS5 Spectrofluorometer

Fluorescence microscopy is an imaging technique that uses fluorescence, either by intrinsic emission or artificially added fluorophores, to provide contrast to microscope images. In biomedical imaging it offers a high degree of specificity and selectivity thanks to the use of multiple fluorescence labelling where different fluorophores can be used to simultaneously identify specific target molecules and cellular structures.

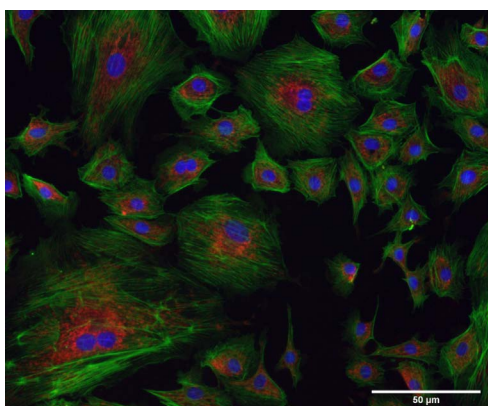


Figure 1: Composite Widefield fluorescence image of bovine pulmonary artery endothelial (BPAE) cells acquired using the FS5 Spectrofluorometer with microscope add-on.

Fluorescence microscopy enables detailed cellular images like that of bovine pulmonary artery endothelial (BPAE) cells shown in Figure 1. BPAE cells contain angiotensin converting enzyme (ACE), which is a vital component in the regulation of blood pressure by constricting and dilating blood vessels. In this BPAE sample,

the different cell components have been labelled with various colour fluorescent dyes in order to observe the structure of the cells. This technical note shows how a fluorescence image like that of BPAE above, along with emission spectra and lifetime decays, can be acquired using an Edinburgh Instruments FS5 Spectrofluorometer with the microscope add-on.

### Experimental Setup

The sample investigated was FluoCells™ Prepared Slide #1 from Invitrogen™ which contains bovine pulmonary artery endothelial (BPAE) cells. The BPAE cells are stained with a combination of fluorescent dyes, each targeting a specific structure in the cell. MitoTracker® Red CMXRos is used to give red emission to mitochondria, Alexa Fluor® 488 phalloidin to give green emission to the filamentous F-actin network, and blue emitting DAPI to label the nuclei.



Figure 2: FS5 Spectrofluorometer coupled to a fluorescence microscope.

All measurements were acquired using an Edinburgh Instruments FS5 coupled to a Nikon Ni-U Upright Fluorescence Microscope. The FS5 was fitted with the

SC-50 Liquid Light Guide Launcher and the excitation and emission light were coupled to and from the microscope using liquid light guides. The FS5 was equipped with a 150W Xenon lamp for steady-state excitation, Time-Correlated Single Photon Counting (TCSPC) lifetime electronics, and a PMT-980 detector. The microscope was equipped with a CMOS fluorescence imaging camera for widefield fluorescence imaging, an epi-fluorescence excitation light guide coupler, an emission light guide coupler, and a laser excitation coupler with an EPL-375 pulsed diode laser.

### Fluorescence Widefield Imaging

To acquire the widefield fluorescence images of the BPAE cells the FS5 and microscope were configured as shown in

Figure 3. The excitation light is supplied by the Xenon lamp of the FS5, and the desired excitation wavelength selected using the excitation monochromator coupled into the excitation liquid light guide using the SC-50 sample module. The excitation light is coupled into the microscope using the widefield excitation coupler, reflected off a dichroic mirror and into the objective lens to excite the sample. The fluorescence from the sample is collected by the objective, transmitted by the dichroic mirror, passed through an emission bandpass filter to select the desired fluorescence wavelength, and imaged using the CMOS camera.

The BPAE cells are labelled with three separate colour fluorescent dyes to visualise the different organelles in the cell. To obtain a complete image of the

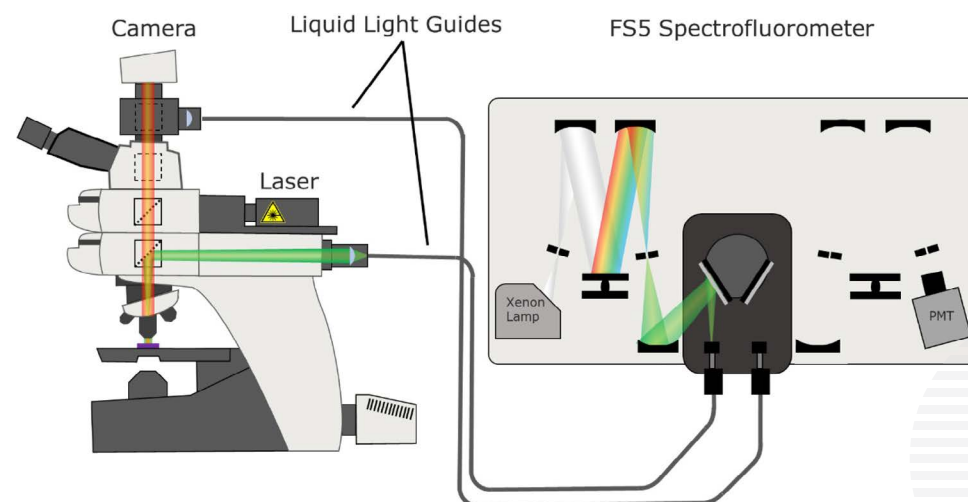


Figure 3: FS5 and microscope configuration for widefield imaging.

cells, three separate images of BPAE were acquired using different excitation wavelengths, dichroic filters and bandpass filters optimised for each dye. Figures 4a - 4c show the individual widefield images of the Alexa Fluor® 488 labelled filamentous F-actin, MitoTracker® Red CMXRos labelled mitochondria, and the DAPI labelled nuclei. These individual images were then combined to give the composite image shown in Figure 4d that reveals the complete structure.

The Xenon lamp and excitation monochromator of the FS5 provide a fully tuneable excitation from 200 to 1000 nm; this gives the user more flexibility compared to the filter-based wavelength selection of excitation sources in traditional microscopy. The excitation monochromator and liquid light guide coupling avoids the common disadvantages that arc lamps have when used as fluorescence microscopy light sources; like the need for the lamp to be aligned or the risk that the lamp heat can damage the sample.

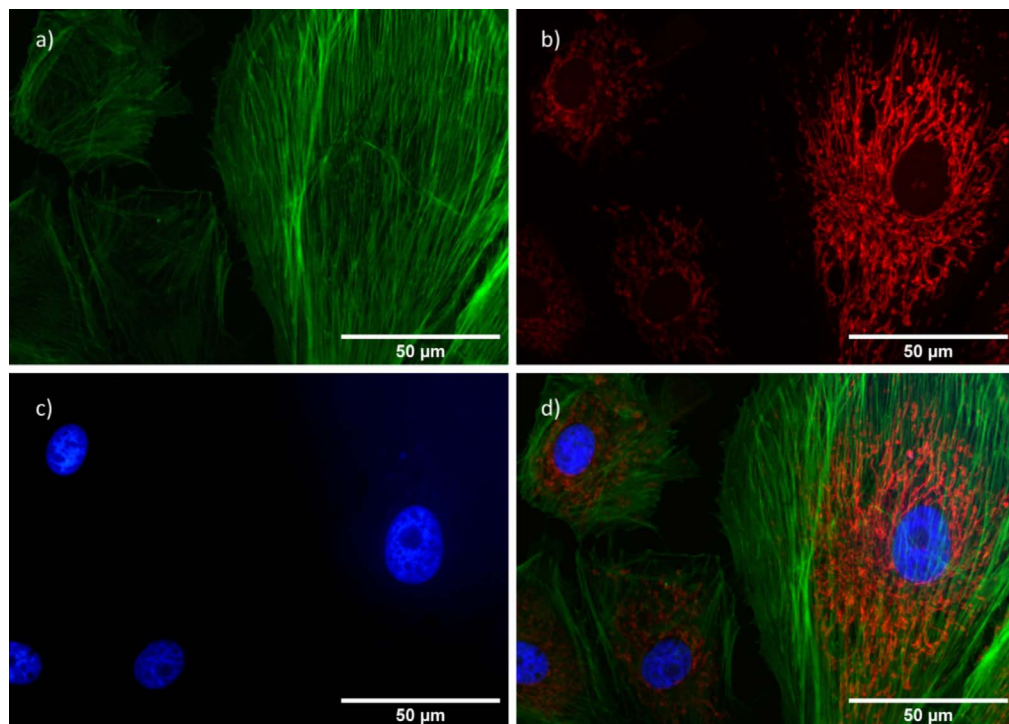


Figure 4: Widefield fluorescence image of bovine pulmonary artery endothelial (BPAE) cells. a) Green emitting filamentous F-actin,  $\lambda_{ex} = 480$  nm with a  $520 \pm 14$  nm emission bandpass. b) Red emitting mitochondria,  $\lambda_{ex} = 580$  nm with a  $641 \pm 38$  nm emission bandpass. c) Blue emitting nuclei,  $\lambda_{ex} = 380$  nm with a  $447 \pm 35$  nm emission bandpass. d) Composite image of BPAE (combination of images a, b, and c)

## Fluorescence Spectra

The spectra of the fluorescence emission from the BPAE cells were measured by re-directing the fluorescence into the emission liquid light for detection using the FS5 as shown in Figure 5. Using this approach, the DNA-bonded DAPI in the nuclei of the BPAE cells was excited at 380 nm and the fluorescence spectrum acquired as shown in Figure 6.

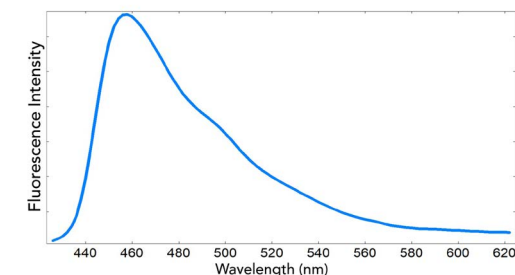


Figure 6 Fluorescence spectrum of DNA-bonded DAPI.

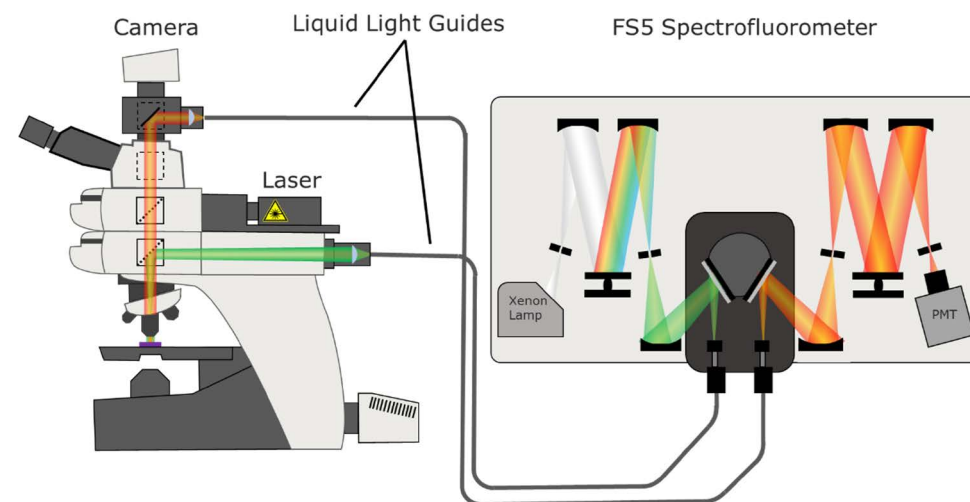


Figure 5: FS5 and microscope configuration for spectral measurements.

## Fluorescence Lifetime

The FS5 with microscope add-on can also be used to acquire the fluorescence lifetime of the labelled BPAE cells. For fluorescence lifetime measurements a pulsed diode laser source is mounted on the microscope using the laser excitation coupler as shown in Figure 7. The camera and microscope stage are used to focus the laser beam to a particular point of interest in the sample. The desired emission wavelength is selected using the emission monochromator of the FS5 and the fluorescence decay acquired using TCSPC.

Using the configuration shown in Figure 7 an EPL-375 pulsed diode was used to excite DNA-bonded DAPI in a nucleus, and the fluorescence decay acquired at 460 nm using TCSPC which is shown in Figure 8. The decay was fit using the Fluoracle<sup>®</sup> operating software of the FS5 which showed an average lifetime of 1.85 ns.

## Conclusion

The FS5 Spectrofluorometer with microscope add-on was used to investigate fluorescently labelled BPAE cells. Using the FS5 Xenon lamp as a continuous range excitation source, widefield fluorescence images of the cells were acquired, revealing the internal structures and features of the cells. Further insight into the properties of fluorescent labels was obtained by measuring their fluorescent spectra and lifetime. This technical note highlights the measurement versatility of the FS5 when equipped with the microscope add-on; being able to acquire images, spectral and lifetime information which together provide a greater understanding of the properties of the sample.

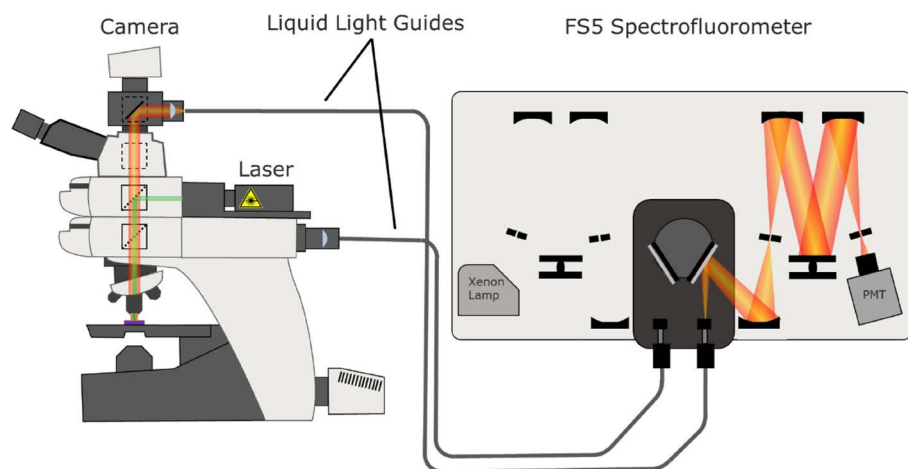


Figure 7: FS5 and microscope configuration for lifetime measurements.

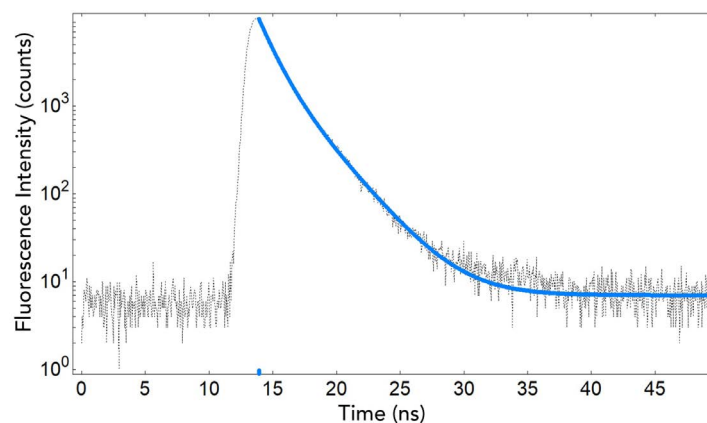
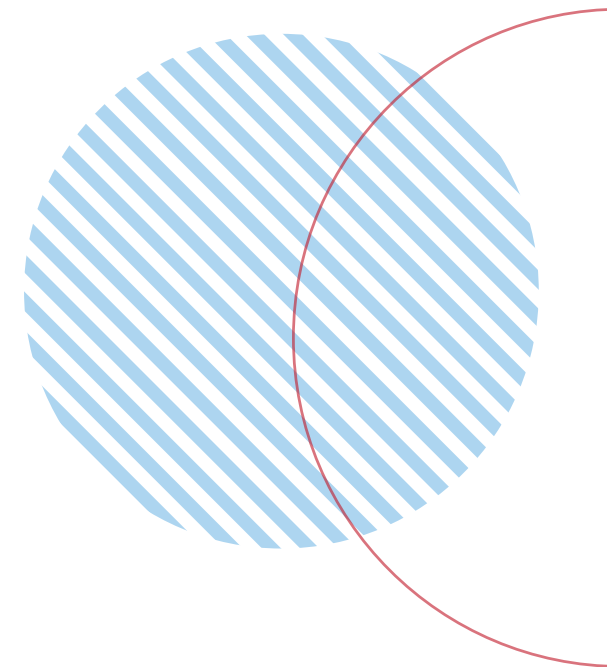


Figure 8: Fluorescence decay of DNA-bonded DAPI acquired using TCSPC.



# Molecular Beacon Probe Fluorescent Detection of DNA

## Key Highlights

- Molecular beacon probes are a sequence of nucleotides that can be used to detect the presence of a specific sequence of DNA or RNA.
- Fluorophore and fluorescence quencher are attached to either end of probe for reaction monitoring.
- By monitoring the change in fluorescence from the fluorophore the presence of specific DNA and RNA sequences can be identified and quantified.

# Molecular Beacon Probe Fluorescent Detection of DNA

## Introduction

Molecular beacon probes are a sequence of nucleotides (the building blocks of DNA and RNA) that can be used to fluorescently detect the presence of a specific sequence of DNA or RNA. The molecular beacon (Figure 1) is designed so that a small number of nucleotide bases (between 5 and 7) at the sequence terminals are complementary to each other and get paired forming what is called the stem. The formation of the stem creates a loop of the unpaired bases, which is termed the stem-loop or hairpin loop. Finally, at one end of the nucleotide sequence there is a covalently attached fluorophore and a fluorescence quencher at the other end of the sequence. When the molecular beacon is in this hairpin form, the quencher heavily diminishes the fluorophore fluorescence through Förster Resonance Energy Transfer (FRET) quenching.

A nucleotide sequence with complementary bases to the molecular beacon loop is called complementary DNA (cDNA). In the presence of its cDNA, the molecular beacon hairpin will open and hybridize with the cDNA to form a double stranded sequence (Figure 2). This hybridization results in the quencher and fluorophore moving further apart so that the fluorophore emission is no longer quenched. By monitoring the change in fluorescence from the fluorophore the presence of cDNA can be identified and quantified.

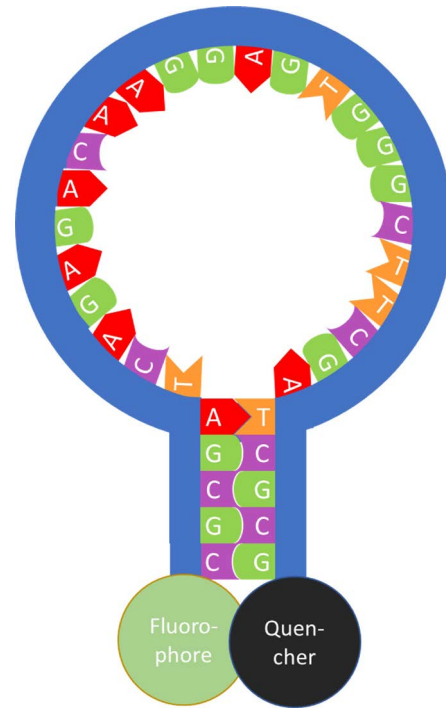


Figure 1: Molecular beacon probe

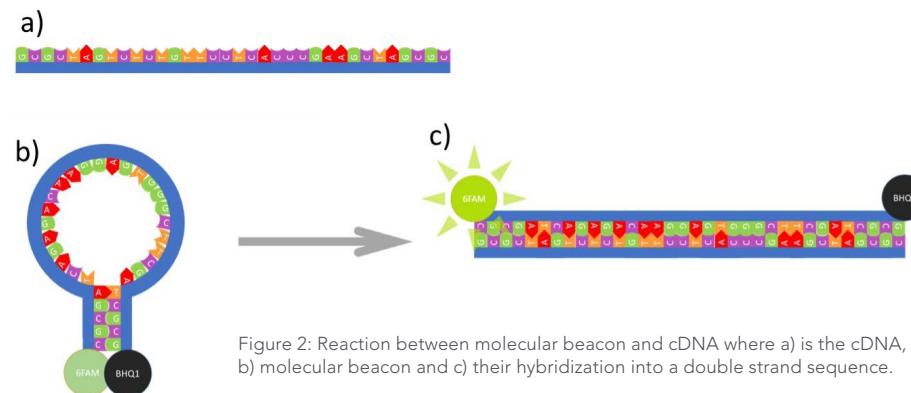


Figure 2: Reaction between molecular beacon and cDNA where a) is the cDNA, b) molecular beacon and c) their hybridization into a double strand sequence.

Molecular beacon probes can be custom designed to target specific DNA or RNA sequences, which allows molecular beacons to be used for real-time detection and quantification of DNA and RNA. Some real-world examples are PCR quantification, in vivo RNA detection, pathogen detection, viral load quantification and study nucleic acid-protein interactions. The use of molecular beacons, coupled with a sensitive spectrofluorometer and sample temperature control, facilitates the measurement of extremely low concentrations of DNA or RNA. In this application note, nanomolar concentrations of cDNA were quantified using a molecular beacon while controlling the temperature of incubation and measuring the sample emission with an Edinburgh Instruments FS5 Spectrofluorometer.

## Experimental Setup

The molecular beacon and its cDNA were purchased from Merck. All measurements were acquired using an Edinburgh Instruments FS5 Spectrofluorometer

equipped with the SC-27 4-Position Temperature Control sample module. The SC-27 was used to heat, while individually stirring, four solutions with different concentrations of cDNA and the molecular beacon. The beacon was excited using the FS5's xenon lamp and its fluorescence detected using a PMT detector. Four solutions were analysed with a molecular beacon concentration of 100 nM and varying concentrations of cDNA: 0 nM, 20 nM, 40 nM, and 60 nM.

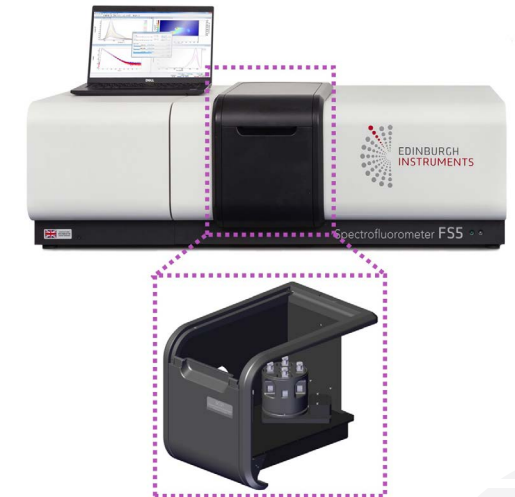


Figure 3: FS5 Spectrofluorometer with SC-27 sample holder

## Temperature Dependence of Hairpin Opening

Hybridization between the cDNA and molecular beacon can occur while the beacon is in the closed hairpin form but will proceed slowly. The hybridization can be accelerated by heating the molecular beacon to first open the hairpin structure. When heated the attraction between the stem base pairs of the hairpin structure is overcome, which is referred as denaturation or melting, and the hairpin opens. The temperature dependence of this opening can be studied using temperature dependent fluorescence, Figure 4.

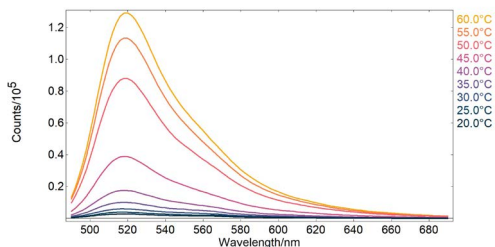


Figure 4: Molecular beacon fluorescence intensity at different temperatures.

The FS5 Fluoracle software can automatically acquire temperature maps when a temperature-controlled sample module is used. The fluorescence temperature map, Figure 4, was acquired by heating the sample at each temperature for 20 minutes while stirring to ensure homogeneous heating of the sample, after the 20 minutes, the emission spectrum was measured before moving to the next temperature. It can be seen that the fluorescence intensity increases with temperature due to the hairpin opening and a reduction in FRET

quenching. 60°C was found to be an adequate temperature for the hairpins to be completely open, with the emission at 60°C being 50 times higher than at 20°C. Based on these results 60°C was chosen as the incubation temperature for DNA detection.

## DNA Detection

Four solutions of the molecular beacon with different cDNA concentrations were pipetted into cuvettes and placed in the four positions of the SC-27. To facilitate hybridization of the cDNA and beacon sequences, the solutions were incubated by heating at 60°C and holding at this temperature for 20 minutes. Then cooled back to 20°C and held at this temperature for a further 20 minutes. This incubation process of heating and cooling increases the hybridization rate between the molecular beacon and cDNA and is illustrated in Figure 5.

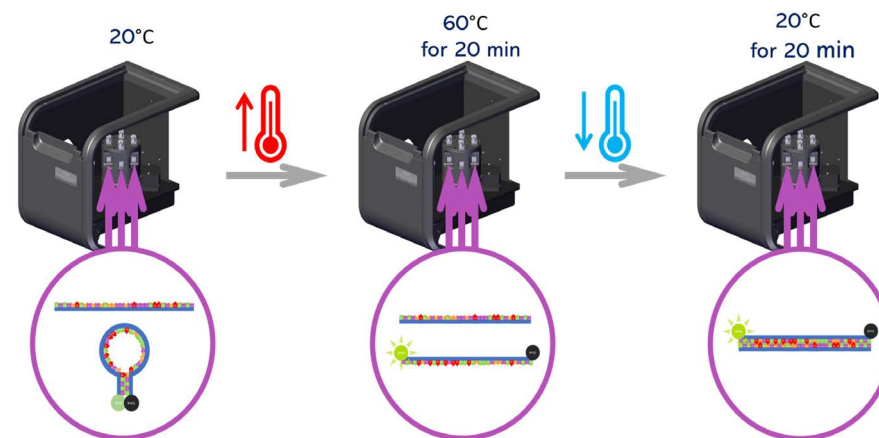


Figure 5: Schematic of the cDNA and molecular beacon hybridization incubation procedure in the SC-27.

The fluorescence spectra of the four solutions after incubation were measured sequentially and shown in Figure 6. The SC-27 enables the automated measurement of four samples with the same measurement parameters. It can be seen that the molecular beacon only solution shows its characteristic emission even without any presence of cDNA, which is due to a small amount of the fluorophore being free in the solution. As the concentration of cDNA is increased, the fluorescence intensity increases due to beacons hybridizing with the cDNA and the fluorophores on the beacon becoming unquenched.

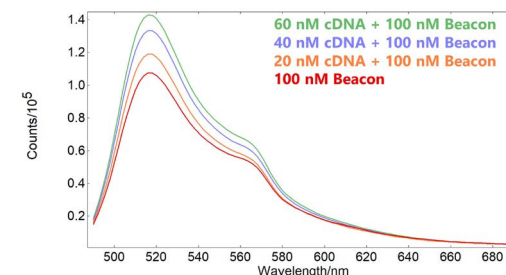


Figure 6: Fluorescence spectra of the molecular beacon solutions in the presence of different concentrations of cDNA

Knowing the fluorescence intensity of samples of known cDNA concentration allows a mathematical correlation between the fluorescence intensity and cDNA to be established. Using the Trend Analysis feature of Fluoracle®, the measurements in Figure 6 were used to create a calibration curve relating the emission intensity at the 516 nm peak to the cDNA concentration (Figure 7).

The following linear relationship between the cDNA concentration and fluorescence intensity was found:

$$Y = 1.076 \times 10^5 + 6.024 \times 10^2 X$$

where Y is the fluorescence intensity at 516 nm, and X is the cDNA concentration in nM.

From this mathematical correlation, the concentration of cDNA in an unknown sample can be determined from its fluorescence intensity. To demonstrate this, a sample with 100 nM molecular beacon concentration and an unknown concentration of cDNA was incubated and the fluorescence at 516 nm measured, which returned a cDNA concentration of 27 nM (Figure 8).

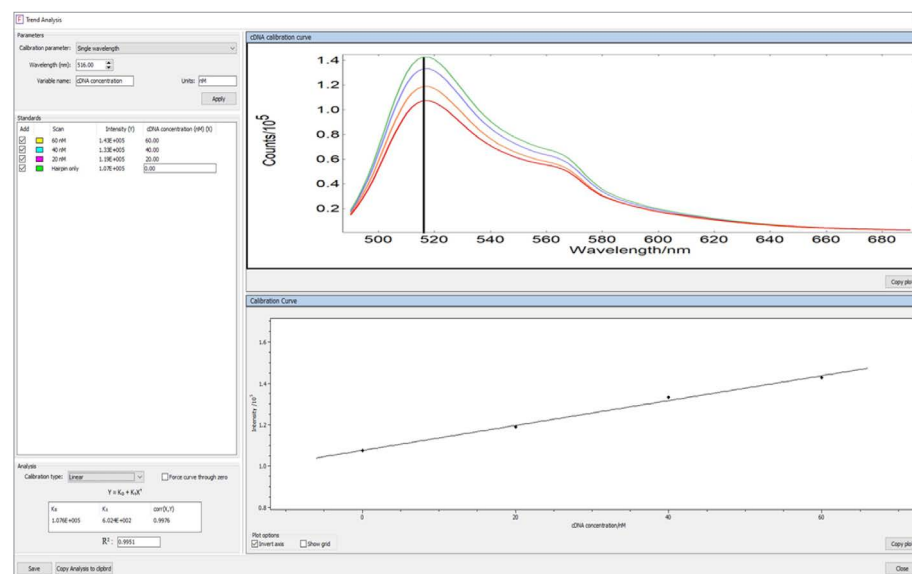


Figure 7: cDNA concentration trend analysis

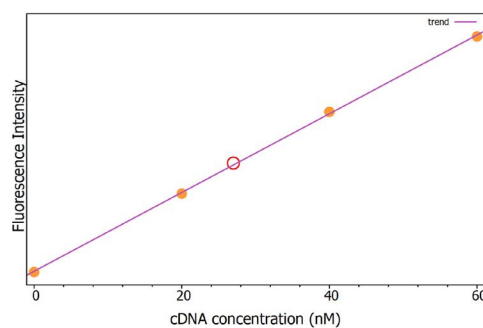


Figure 8: Calibration curve with cDNA known concentration samples (orange dots) and unknown cDNA concentration sample (red circle).

## Conclusion

An Edinburgh Instruments FS5 Spectrofluorometer was used to determine an unknown concentration of DNA, in the order of nanomolar, using a molecular beacon probe. The DNA and probe solutions were incubated using the SC-27 Four Position Temperature Controlled Sample Module and the measurement of the fluorescence intensity of the four solutions automated. The results were analysed using the Trend Analysis feature of the FS5 Fluoracle® software.



# ATR-FTIR of Blood Serum

## Key Highlights

- ATR-FTIR can provide rapid 'biofluid biopsies'.
- Detailed fingerprint spectral analysis can differentiate between healthy and diseased samples.
- Using a heated ATR accessory removes water interference quickly.

## ATR-FTIR of Blood Serum

### Introduction

Attenuated total reflection Fourier transform infrared (ATR-FTIR) spectroscopy is a fantastic technique for analysing biofluids. By measuring molecular bond vibrations when interrogated with IR light a biological fingerprint can be obtained from the sample in the form of an IR spectrum. 'Biofluid biopsies' are of interest to healthcare researchers and clinicians because they represent a minimally invasive sample collection method. Many biofluids, such as urine, saliva, and blood, can be studied using ATR-FTIR. Spectral differences between biofluid samples allows differentiation between healthy and diseased patients.

Blood is the most widely used biofluid in diagnostic medicine, it is composed of plasma, red blood cells, white blood cells, and platelets. For spectroscopic analysis, plasma, or serum is typically used, this is because both solutions can be frozen for preservation. In whole blood the freezing process would result in cell disruption and the haemoglobin has a large spectral influence. Plasma is an aqueous solution which is separated by centrifuging in an anti-coagulant tube, while serum is created by separating the blood cells and platelets by allowing the blood to clot, Figure 1. Serum is more commonly used as this preparation method is more efficient at removing red blood cells.

ATR-FTIR in the mid-IR region ( $4000\text{ cm}^{-1}$  –  $400\text{ cm}^{-1}$ ) contains the fundamental vibrations of the functional groups in biological samples, such as proteins, lipids, and amino acids.

The technique requires a small sample volume in the order of microlitres providing rapid results whilst also being a cost-effective and easy-to-use method for diagnostics. Serum analysis using ATR-FTIR spectroscopy has been demonstrated for a number of disease studies such as cancer, endometriosis, brain disorders, and viral infections.<sup>1-6</sup>

### Impact of Water on Biofluid Measurements

One drawback of ATR-FTIR for biofluid analysis is the influence of water on the IR spectrum, Figure 2. Water produces a strong IR response due to its polarity, and when biofluids are analysed in liquid phase using ATR-FTIR the water spectrum masks the biological information from the sample. Standardly, when measuring biofluids, the user must wait for the sample to dry and reveal the biological spectrum, however, this is time-consuming and slows down the total acquisition time. A faster approach is to use a heated ATR accessory. By heating the sample, the water will evaporate faster, and the total acquisition time is significantly reduced. In this application note, an IR5 FTIR Spectrometer equipped with the heated ATR accessory was used to remove water and rapidly measure the spectrum of serum.

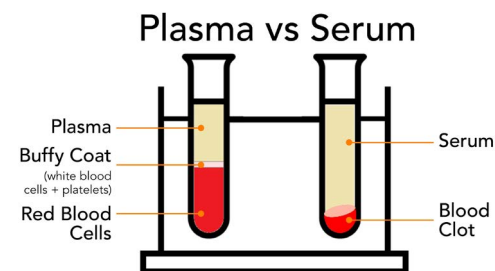


Figure 1: Plasma vs serum.

### Materials & Methods

A sample of Human serum albumin was measured in an Edinburgh Instruments IR5 FTIR Spectrometer equipped with a heated ATR accessory, Figure 3. The ATR's internal reflective element (IRE) was diamond, a commonly used IRE due to its high refractive index and robustness. As a result of their excellent thermal conductivity diamond ATRs are particularly suited to heated experiments.

To demonstrate the effect that heating the ATR has on drying times,  $3\text{ }\mu\text{L}$  of sample was pipetted onto the ATR without heating and spectra were collected. This process was repeated with the ATR pre-heated and held constant at  $50^\circ\text{C}$ . The IR spectra were collected with a resolution of  $4\text{ cm}^{-1}$  averaging 10 spectra with a total acquisition time of 35 seconds for each spectrum.

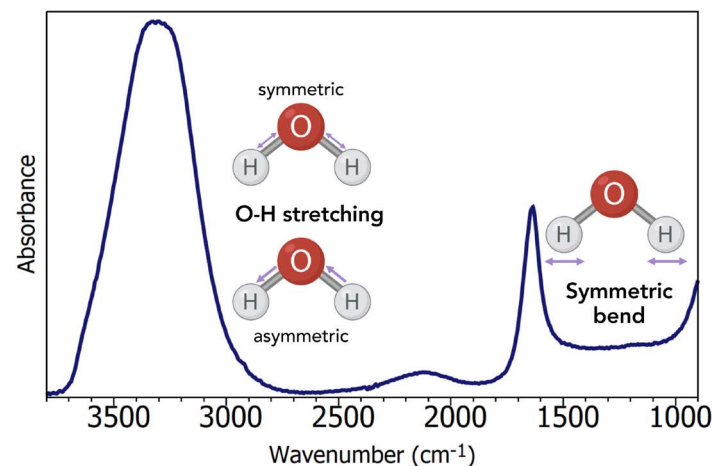


Figure 2: ATR-FTIR spectrum of water.

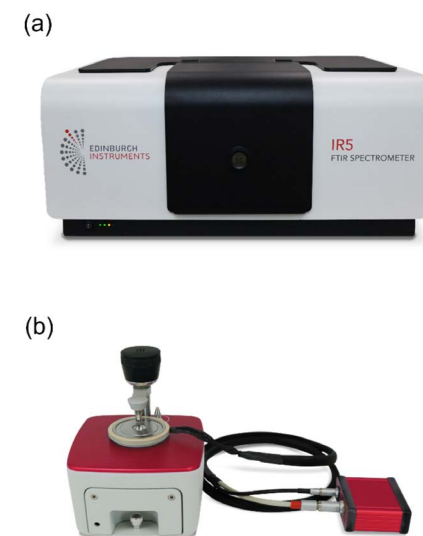


Figure 3: Edinburgh Instruments IR5 FTIR Spectrometer (a) and heated ATR accessory (b).

## Results & Discussion

The IR spectra of Human serum albumin acquired after 2 minutes drying on a room temperature (blue) and heated (red) ATR are shown in Figure 4. In the room temperature ATR measurement, the spectrum is dominated by the strong water absorption bands and the biological spectrum is obscured. While for the heated ATR a full biological spectrum without any water interference was obtained. If the blue spectrum was left to dry longer at room temperature it would take over 15 minutes of drying for the biological spectrum to be sufficiently revealed for analysis, greatly reducing measurement throughput.

ATR-FTIR reveals significant information on the biological components within a biofluid sample and Figure 5 gives the band assignments of the serum spectrum. IR bio-spectra can be thought of as two regions: the high-wavenumber region from  $2600\text{ cm}^{-1}$  to  $3800\text{ cm}^{-1}$ , and the low-wavenumber region from  $2000\text{ cm}^{-1}$  to  $500\text{ cm}^{-1}$  consisting of double bond stretching and the fingerprint region. The low-wavenumber region produces the most discriminatory data, and is the area most used for diagnostics.<sup>7</sup>

## Conclusion

This application note demonstrates the high sensitivity of the IR5 to the analysis of biofluids by providing a biological fingerprint of a serum sample. The problem of parasitic water absorption was overcome by equipping the IR5 with a heated ATR accessory. By using a heated ATR the drying time required before spectral acquisition was greatly reduced without reducing the spectral quality.

## References

1. T. Soares Martins *et al.*, "Potential of FTIR Spectroscopy Applied to Exosomes for Alzheimer's Disease Discrimination: A Pilot Study," *J. Alzheimer's Dis.*, vol. **74**, no. 1, pp. 391–405, 2020.
2. L. J. Pabico *et al.*, "Diagnostic Efficiency of Serum-Based Infrared Spectroscopy in Detecting Breast Cancer: A Meta-Analysis," *Lab. Med.*, vol. **54**, no. 1, pp. 98–105, 2023.
3. S. Guo *et al.*, "Fast and Deep Diagnosis Using Blood-Based ATR-FTIR Spectroscopy for Digestive Tract Cancers," *Biomolecules*, vol. **12**, no. 12, pp. 1–15, 2022.
4. S. Roy *et al.*, "Spectroscopy goes viral: Diagnosis of hepatitis B and C virus infection from human sera using ATR-FTIR spectroscopy," *Clin. Spectrosc.*, vol. **1**, p. 100001, 2019.
5. K. Naseer *et al.*, "ATR-FTIR spectroscopy as the future of diagnostics: a systematic review of the approach using bio-fluids," *Appl. Spectrosc. Rev.*, vol. **56**, no. 2, pp. 85–97, 2021.
6. I. Kokot *et al.*, "ATR-IR Spectroscopy Application to Diagnostic Screening of Advanced Endometriosis," *Oxid. Med. Cell. Longev.*, vol. **2022**, 2022.
7. A. Rohman *et al.*, "The use of FTIR and Raman spectroscopy in combination with chemometrics for analysis of biomolecules in biomedical fluids: A review," *Biomed. Spectrosc. Imaging*, vol. **8**, no. 3–4, pp. 55–71, 2019.

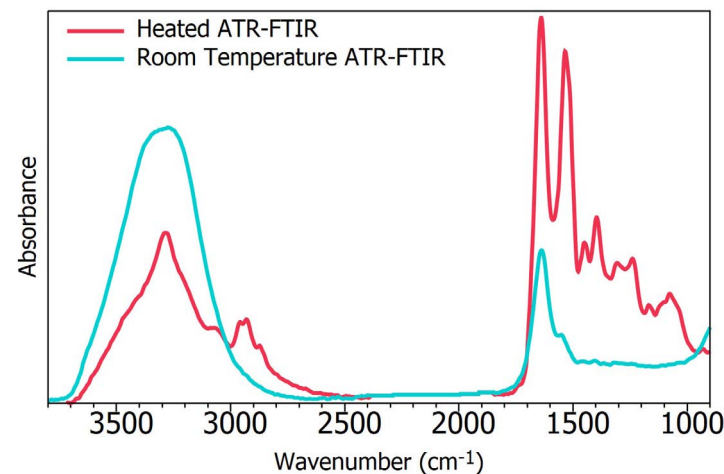


Figure 4: ATR-FTIR spectra after 2 minutes drying time of Human serum albumin at room temperature (blue) and heated to  $50^{\circ}\text{C}$  (red).

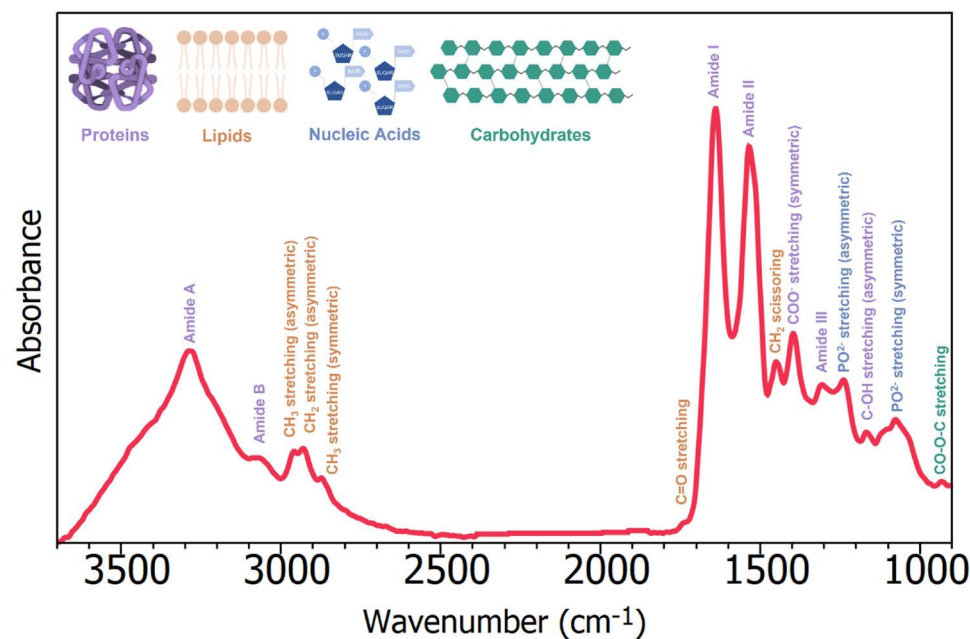


Figure 5: ATR-FTIR spectrum with band assignments of Human serum albumin.



EDINBURGH  
INSTRUMENTS